Heat-Capacity Measurements on Manganese Dibromide Tetrahydrate near Its Néel Temperature*†

R. D. Hempstead‡ and J. M. Mochel
Department of Physics and Materials Research Laboratory, University of Illinois, Urbana, Illinois 61801
(Received 8 November 1971)

Heat-capacity measurements on very small single crystals of manganese dibromide tetrahydrate have been made using the ac or oscillating-temperature method. These measurements show rounding in a temperature range of about 1 mK at the Néel temperature (2.12 K). We believe this rounding is due to chemical impurities. Outside this region the data may be fitted by a power-law singularity, within the experimental error, with $0.08 \leq \alpha \leq 0.23$, $-0.10 \leq \alpha' \leq 0.03$, and $2.1195 \leq T_N \leq 2.1203$ K. The errors in α, α', and T_N were obtained from a χ^2 test for 90% probability that the true values lie within these limits. Comparison is made to the heat-capacity measurements by Dixon and Rives on $MnCl_2 \cdot 2H_2O$, which is nearly isostructural to $MnBr_2 \cdot 4H_2O$. The heat capacity in the critical region of partially deuterated crystals with 1% deuterium was measured to obtain the effect of this impurity on the rounding. No significant effect was observed.

I. INTRODUCTION

It is well known that the heat-capacity singularity at a second-order phase transition is not a simple step discontinuity as predicted by the mean-field theories.[1] Instead, the heat-capacity anomalies of the liquid-gas critical point and the order-disorder transition of β-brass[2] seem to fit phenomenological power-law singularities of the form

$$C = (A/\alpha)[\,|\epsilon|^{-\alpha} - 1] + B \quad \text{for } T > T_c$$
$$= (A'/\alpha')[\,|\epsilon|^{-\alpha'} - 1] + B' \quad \text{for } T < T_c\,, \qquad (1)$$

where

$$\epsilon = (T - T_c)/T_c \qquad (2)$$

is the reduced temperature (T_c is the transition temperature), A, B, A', and B' are constants; and α and α' are constants which are called the critical exponents. Theoretical calculations on various forms of the Ising and Heisenberg models also show heat-capacity singularities of the above form.[3] Heat-capacity measurements on magnetic systems,[1] however, seldom show this ideal power-law divergence. Rather, most heat-capacity data can be fitted to a power-law divergence only for some range of $|\epsilon|$. For large $|\epsilon|$ ($> 10^{-1}$–10^{-2}), we expect that magnetic systems are not in the critical region, and hence their heat capacity would not be expected to follow a power-law singularity.[4] However, for small $|\epsilon|$ (10^{-4}–10^{-3}, depending on the system) deviations from a power-law singularity are presently not well understood. This deviation is usually called rounding since it takes the form of rounding the singularity.

We have studied the antiferromagnetic transition in $MnBr_2 \cdot 4H_2O$, which has a Néel temperature of 2.12 K. This transition temperature is very convenient because of its easy access by pumping on liquid He[4]. Also, in this temperature range the lattice and background heat capacities are small and can be considered to be included in the constants B and B' when the heat-capacity data are fitted to Eq. (1). Our measurements can be compared to the heat-capacity measurements of Dixon and Rives on $MnCl_2 \cdot 4H_2O$, which is believed to have the same magnetic structure as $MnBr_2 \cdot 4H_2O$.[5] Also, comparison can be made to the thermal-expansion data of Philip *et al.*[6] on both $MnBr_2 \cdot 4H_2O$ and $MnCl_2 \cdot 4H_2O$. Unfortunately, $MnBr_2 \cdot 4H_2O$ has a very complex magnetic structure, so that comparisons to theoretical calculations are difficult to make.

Since our heat-capacity data on small crystals show the same rounding as observed in large crystals, we tried to introduce impurities into the system to induce more rounding. This was done by growing partially deuterated crystals with 1-mole% heavy water. No additional rounding was observed.

II. PREVIOUS WORK

The antiferromagnetic transtions in $MnBr_2 \cdot 4H_2O$ and $MnCl_2 \cdot 4H_2O$, hereafter referred to as the bromide and chloride, respectively, were first discovered by Henry.[7] Because the bromide and chloride are believed to be nearly isostructural[8] (monoclinic with space group $P2_1/n$), the more extensive studies of the chloride are used to infer various properties of the bromide. Using a unit cell with space group $P2_1/a$, Spence and Nagarajan[9] reported the magnetic space group $P2_1/a'$ for the chloride, which corresponds to parallel spins lying in planes perpendicular to the b axis.

Gijsman *et al.*[10] found both materials to have

easy axes of magnetization along the c axis. Because the free state of Mn^{++} has $S=0$ and the reported g value for the chloride is 2.011,[10] we expect that the anisotropic exchange interaction is negligible.[11] Since the g value is isotropic to within $\frac{1}{2}\%$,[10] we expect that the contribution from the crystalline field to the anisotropy energy is small. Thus the magnetic dipole interaction can add significantly to the anisotropy energy. Evidence of spin flopping in magnetization measurements has been observed for the chloride, but not for the bromide.[10,12] However, antiferromagnetic-resonance measurements[13] and optical-absorption measurements[14] showed evidence of spin flopping in the bromide. Using the results of Bolger[13] for the critical magnetic field to estimate the anisotropy energy and mean-field theory to estimate the superexchange energy, we find that the anisotropy energy for the bromide is about 30% of the superexchange energy.[15]

Heat-capacity measurements on the bromide near its Néel temperature have been made by Kapadnis and Hartmans,[16] Schelleng and Friedberg,[17] and Miedema *et al.*[18] None of these measurements has sufficient temperature resolution to fit the data to a power-law singularity. For the chloride, however, high-resolution heat-capacity measurements have been made by Dixon and Rives.[19]

Thermal-expansion measurements have been made by Philip *et al.*[6] on both the bromide and chloride near their transition temperatures. From recent work[20] on the relationship between the thermal-expansion coefficients and the specific heat, we expect that the critical exponents for a power-law fit to the volume-thermal-expansion coefficient will be the same as those for the specific heat.[21] Dixon and Rives[19] compared their heat-capacity measurements on the chloride to the thermal-expansion data of Philip *et al.* and found that within experimental error they have the same temperature dependence in the critical region.

III. EXPERIMENTAL METHOD

A. Sample Preparation

Crystals for this experiment were grown from a saturated solution of $MnBr_2 \cdot 4H_2O$ obtained from Alfa Inorganic Inc., Beverly, Mass. After several recrystallizations, crystals of dimension roughly 1 mm on a side were grown for these measurements. In addition, crystals of 1 mole% deuterated $MnBr_2 \cdot 4H_2O$ were grown from a saturated solution obtained by dehydrating $MnBr_2 \cdot 4H_2O$ in a vacuum and dissolving the anhydrous $MnBr_2$ in a mixture of 1-mole% heavy water and 90-mole% natural water.

An emission spectrographic analysis showed the following impurity concentrations in ppm by weight: Mg, 300; Al, 80; Ca, 80: Si, 80; Cu, 60; Fe, 40; Ni, 40; and Cr, 30. No other elements were detected. This corresponds to approximately 0.007 impurity atoms for every manganese ion. Hence the typical interimpurity distance along any line in the crystal is 140 spin spacings.

B. Oscillating-Temperature Technique

The method used for these heat-capacity measurements is the ac or oscillating-temperature technique first used at low temperatures by Sullivan and Seidel.[22] In this method the sample is weakly connected to a heat sink through a thermal link of conductance K. A sinusoidal heat input of frequency ω is supplied to the sample. By solving the energy-conservation equation of the sample for the amplitude of its temperature oscillations, we find that this amplitude is inversely proportional to the heat capacity C of the sample, if ω is chosen such that $\omega \gg K/C$. Thus the relative heat capacity can be obtained as a function of temperature by measuring the amplitude of the temperature oscillations.

We have chosen this method rather than the adiabatic method for several reasons. The oscillating-temperature technique enables us to measure the heat capacity of a small single crystal, whereas the adiabatic technique requires a sample with a large heat capacity. Earlier measurements using the adiabatic technique have used polycrystalline samples[23] or large single crystals.[24] Polycrystalline samples are expected to have even more rounding than a single crystal. Furthermore, a large single crystal is more likely to have strains and other crystalline imperfections than a small single crystal. Thus we expect to have the least rounding in a small single crystal.

Because the uncertainties in the fitting parameters of the power-law singularity depend upon the precision of the heat-capacity measurements, and because of rounding, we have tried to maximize the precision of our heat-capacity data rather than maximize the temperature resolution. Since the crystals measured showed rounding over the temperature range of about 1 mK, we have used a resolution of about 100 μK near the Néel temperature. This permits us to obtain measurements with errors less than 1% over the temperature range $10^{-4} \leq |\epsilon| \leq 10^{-1}$. Furthermore, the data can be taken point by point so that the data points can be chosen to have the temperature distribution required by the fitting procedure.

C. Experimental Apparatus

Two slightly different designs were used for heating and measuring the temperature of the crystal. The first, shown in Fig. 1, was used for measurements on the nondeuterated crystals. It

consists of a thermometer and heater on opposite side of a crystal. Thermal contact between the heater and crystal and between the thermometer and crystal was made through Cry-Con grease. Because of the pastelike consistency of Cry-Con grease and in order to maximize the contact surface area, we enclosed this heater-grease-crystal-grease-thermometer assembly in a cylinder made from 0.0005-in. Kapton film wrapped around itself several times. The thermometer consisted of a piece of antimony-doped germanium with dimensions $\frac{1}{8}$ in. square by 0.010 in. thick. Contacts to the germanium were made with 0.0025-in.-diameter Advance wire soldered with Cerroseal using Divco No. 335 flux. The heater was made from a 600-Ω length (about 18 in.) of very-high-resistance wire taken from a wire-wound resistor.[25] The crystal had typical dimensions of 1 mm on a side. An adjustable thermal link to the heat sink was provided by a piece of No. 46 copper wire approximately 1 in. long in series with a piece of 0.005-in.-diameter Advance wire about $\frac{1}{4}$ in. long. This thermal link was varied by changing the length of the Advance part of the wire. Typically, the relaxation time of the crystal temperature to the heat-sink temperature was 300 sec at the transition temperature and 30 sec at $\epsilon = +10^{-1}$.

The sample assembly, shown in Fig. 2, used for measurements on the partially deuterated crystals was slightly different from that described above. Because of excessive noise in the germanium thermometer,[26] a 330-Ω Allen Bradley hot-molded carbon resistor was used for the thermometer. The ceramic coating on the resistor was sanded off on three sides. A piece of 0.0001-in. Mylar film with a 1000-Å copper film evaporated onto it was coated with Apiezon N grease and wrapped around the resistor to provide a thermally conducting jacket. The Kapton-film cylinder was shortened so that it covered only the heater and the top half of the crystal. Apiezon N grease was used for thermal contact rather than Cry-Con. Although N grease has lower thermal conductivity than Cry-Con grease, it was found that N grease provided better thermal contact since it could be more easily handled, making possible thinner layers of grease between the heater and crystal and between the crystal and thermometer.[27]

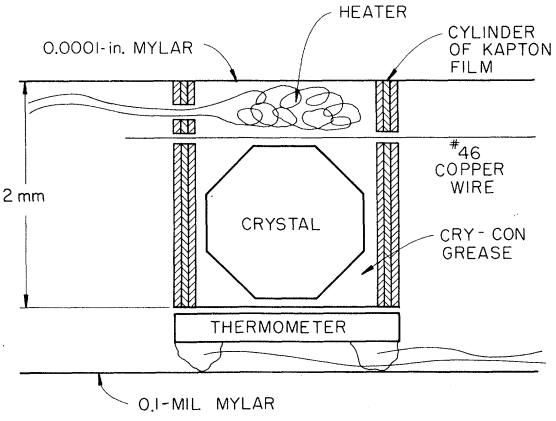

FIG. 1. Sample assembly used for heat-capacity measurements.

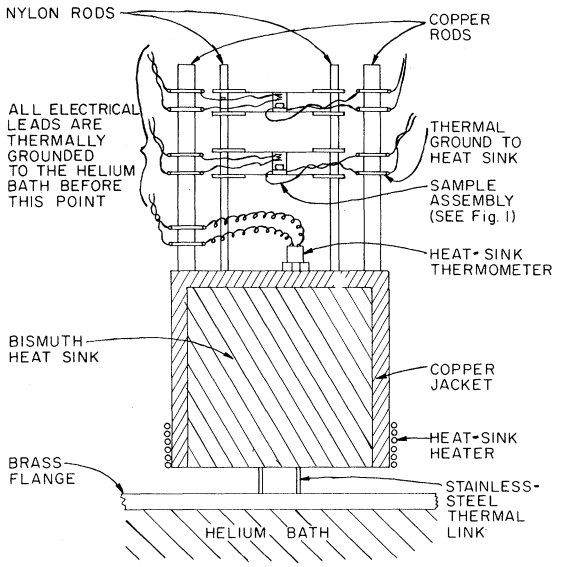

FIG. 2. Insert for heat-capacity measurements.

Our greatest difficulty was in obtaining sufficiently good thermal contact between the heater and crystal and between the crystal and thermometer.

Two sample assemblies of the type discussed above are held between two pieces of 0.0001-in. Mylar film, which is in turn supported by nylon frames and nylon rods mounted on a copper-encased bismuth heat sink. This supporting structure plus the heater and thermometer leads gives about 10% of the total thermal link between the sample assembly and the heat sink. The heat sink is thermally linked to a liquid He^4 bath by a piece of stainless-steel tubing, causing the heat sink to have a thermal relaxation time of about 40 sec at 2 K. A Texas Instruments Type-106 germanium thermometer is mounted on the heat sink and a heater made from 0.002-in. manganin wire, with a total resistance of 600 Ω, is wrapped around the bottom of the heat sink. N grease is used on both for good thermal contact. This thermometer and heater are used in a feedback-control loop, shown in Fig. 3, which is capable of maintaining the heat-sink temperature to within 10 μK of the desired value. The region surrounding the heat sink is evacuated.

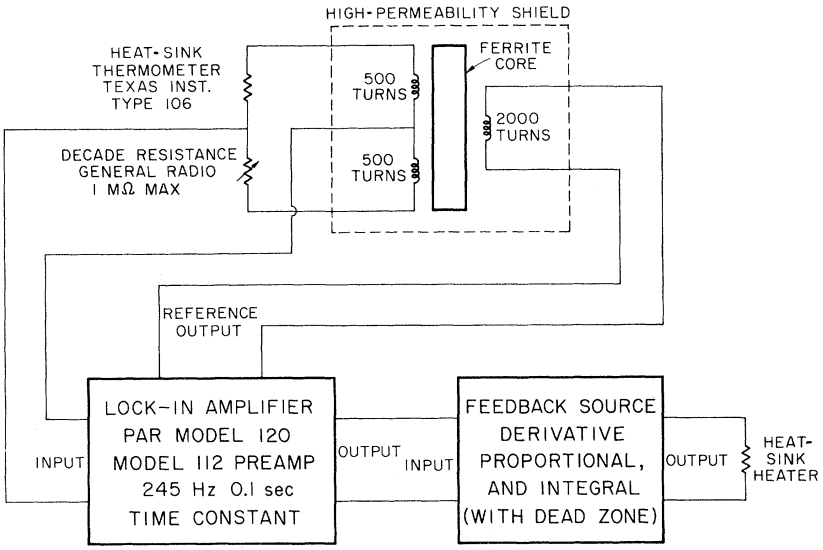

FIG. 3. Block diagram for the temperature-controller circuit.

In Fig. 4 is shown the circuitry used to provide the sinusoidal heat input to the crystal (typically at 0.05 Hz), to measure the crystal's mean temperature, and to measure the amplitude of the temperature oscillations. The ac-bridge network for the thermometer on the crystal is the same as that shown in Fig. 3. Because of the temperature oscillations of the crystals, the output of the lock-in amplifier is oscillating. By setting the decade resistance box to yield symmetric oscillations about zero in the lock-in output, i.e., so that the time-averaged bridge output is zero, we can determine the mean resistance of the thermometer and hence the crystal's mean temperature. The amplitude of these temperature oscillations is measured using a Fabri-Tek Model-1072 signal analyzer as a very-low-frequency lock-in detector. Feeding the output of the lock-in amplifier into the signal analyzer, we trigger the sweep at the start of every other cycle of the temperature oscillation using a trigger signal from the variable-phase output of the Hewlett-Packard Model-203A function generator. The sweep speed of the signal analyzer is set so that two periods of the temperature oscillations correspond to the total sweep time of the signal analyzer. We set the phase of the trigger signal so that the signal analyzer starts its sweep when the temperature is at its mean point. When the averaging is finished (usually after two or four sweeps), we can eliminate any dc background (caused by inexact setting of the decade resistance box to the mean resistance value of the ther-

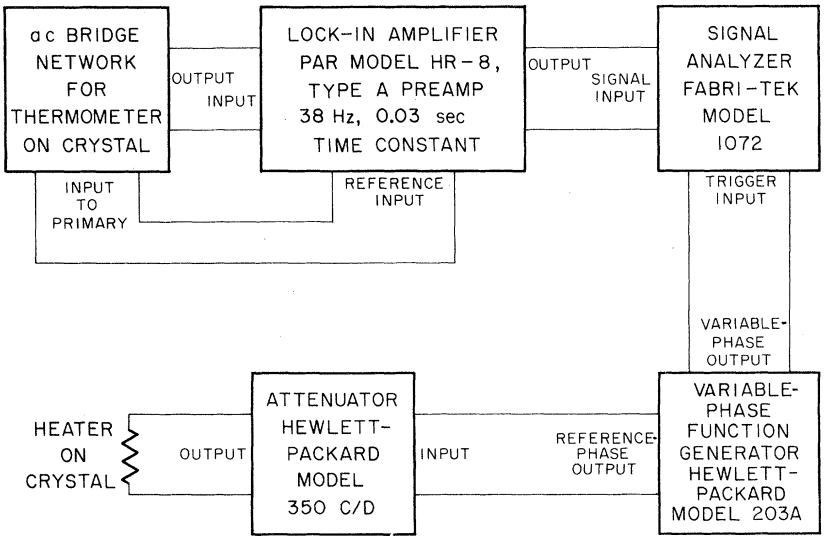

FIG. 4. Block diagram for the circuit used to measure the mean temperature of the crystal and the size of the temperature oscillations.

mometer). This is done by subtracting the contents of the second quarter of the memory from the the first, adding the third, and subtracting the fourth. The half-cycle in the first quarter is then integrated to give a number proportional to the amplitude of the temperature oscillations.

D. Lumped-Parameter Model for the Sample Assembly

We stated above that we required $\omega \gg C/K$; however, there is also an upper frequency limit due to the requirement that the sample assembly be in thermal equilibrium on the time scale of the temperature oscillations. To determine the limiting behavior in this high-frequency limit, we set up a lumped-parameter model. The limiting factors are the thermal contacts between the heater and crystal and between the crystal and thermometer. Also, the parallel thermal path from the heater directly to the thermometer by passing the crystal must be considered, even though it is much weaker than the thermal path through the crystal. We propose, therefore, the model shown in Fig. 5.

In order to obtain the temperature variations as a function of the heat capacities and thermal conductances defined in Fig. 5, we can solve the set of energy-conservation equations for the heater, crystal, and thermometer using the sinusoidal input voltage $V(t) = V_0 \sin(\omega t/2)$ to the heater with resistance R. In the limiting condition $\omega\tau = \omega C/K \gg 1$; $\omega\tau_T = \omega C_T/K_T \ll 1$; $\omega\tau_H = \omega C_H/K_H \ll 1$; $K_{H\text{-}T} \ll K_H, K_T$; and $C \gg C_H, C_T$; the temperature variations as measured by the thermometer are given by

$$\Delta T(t) = \frac{1}{2}\,\frac{V_0^2}{R}\left(\frac{1}{K} + \frac{1}{\omega(C+C_T+C_H)} \times \frac{\sin(\omega t+\theta)}{\{1+[\omega\tau_H+\omega\tau_T-(K_{H\text{-}T}\omega C/K_T K_H)-(1/\omega\tau)]^2\}^{1/2}}\right), \tag{3}$$

where θ is given by

$$\theta = \pi - \tan^{-1}\left(\omega\tau_H+\omega\tau_T-\frac{K_{H\text{-}T}\omega C}{K_T K_H}-\frac{1}{\omega\tau}\right). \tag{4}$$

Thus our lumped-parameter model predicts that we can measure the total heat capacity to a 1% accuracy if we satisfy the condition

$$\left|\omega\tau_H+\omega\tau_T-\frac{K_{H\text{-}T}\omega C}{K_T K_H}-\frac{1}{\omega\tau}\right| \leq \frac{1}{7}. \tag{5}$$

In order to find the proper operating frequency and to show that the above condition is satisfied, we measure the transient response of the system to a voltage pulse. Solving the energy-conservation equations in the same limit for a voltage pulse of height V_0 and width Δt, we obtain

$$\Delta T(t) = \frac{1}{2}\,\frac{V_0^2}{R}\,\frac{K_{H\text{-}T}}{C_H C_T}\,t^2 \quad \text{for } 0 < t < \Delta t, \tag{6}$$

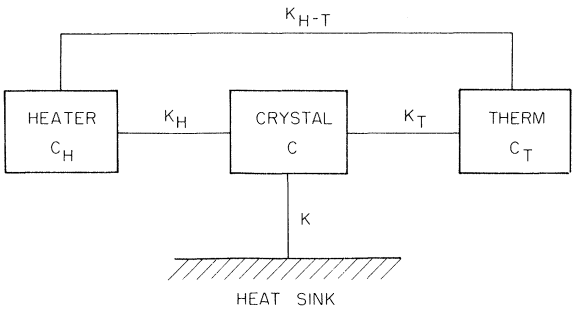

FIG. 5. Lumped-parameter model for the sample assembly. K, K_H, K_T, and $K_{H\text{-}T}$ are the thermal conductances of the thermal links shown. C_H, C, and C_T are the heat capacities of the components shown.

$$\Delta T(t) = \frac{V_0^2 \Delta t}{RC}\left[e^{-(t-\Delta t)/\tau} + \left(\frac{K_{H\text{-}T}C\Delta t}{2C_H C_T}-1\right)e^{-(t-\Delta t)/\tau_T}\right] \quad \text{for } t > \Delta t, \tag{7}$$

where we have assumed $\tau_T \gtrsim \tau_H$ and $\Delta t \ll \tau_H$. If $K_{H\text{-}T}C\Delta t/2C_H C_T < 1$, after Δt we have an exponential rise of time constant τ_T followed by a slower exponential decay of time constant τ. If $K_{H\text{-}T}C\Delta t/2C_H C_T > 1$, we have an overshoot of the temperature of the thermometer above the temperature of the crystal during the pulse due to the bypass heat current through $K_{H\text{-}T}$. After the pulse this overshoot decays exponentially with time constant τ_T, followed by a slower exponential decay of time constant τ. The worst case for overshoot is at the transition temperature where the crystal's heat capacity is maximum. To see how this relates to the steady-state response, we can substitute $\Delta t \lesssim \tau_H$ and $\omega < \frac{1}{7}\tau_T$ into the overshoot condition to obtain the same condition on $K_{H\text{-}T}$, as required by Eq. (5).

Thus, to ensure that our heat-capacity measurements were 1% accurate, we measured the transient response at the heat-capacity maximum to make sure there was no overshoot, and we measured the transient response at the highest temperature at which measurements were made (2.31 K) to obtain τ_T and the minimum value of $\tau(\tau_{\min})$. The operating frequency was then chosen to satisfy the condition for 1% accuracy:

$$7/\tau_{\min} \leq \omega \leq \tfrac{1}{7}\tau_T. \tag{8}$$

IV. DATA ANALYSIS

A. Calibration of Raw Data

The heat-sink thermometer was calibrated against the vapor pressure of He^4 using a Texas Instruments fused-quartz precision gauge to mea-

sure the pressure. The resulting resistance-vs-temperature data were then fitted to the functional form[28]

$$1/T = C_{-1}(\ln R)^{-1} + C_0 + C_1 \ln R + C_2(\ln R)^2 + C_3(\ln R)^3 , \tag{9}$$

where the constants C_{-1}, C_0, C_1, C_2, and C_3 were determined by a least-squares-fitting procedure. The errors of this fitting function from the calibration data were less than 1 mK, whereas the accuracy of the calibration data was about 2 mK. This calibration was done once and used for all runs. We expect that absolute-temperature comparisons from run to run are limited to about 0.5 mK.[29] The thermometer on the crystal was then calibrated for each run against the thermometer on the heat sink and fitted to the same functional form.

The size of the temperature oscillations can be obtained from the size of the voltage oscillations ΔV, the sensitivity of the bridge $(dR/dV)^{-1}$, and the sensitivity of thermometer $(dT/dR)^{-1}$:

$$\Delta T = \Delta V \frac{dR}{dV} \frac{dT}{dR} . \tag{10}$$

The sensitivity of the thermometer is obtained by differentiating the fitting function [Eq. (9)]. The sensitivity of the bridge as a function of the thermometer's resistance R is given by

$$\frac{dR}{dV} = \frac{R}{V}\left(1 + \frac{R}{2R_D}\right) , \tag{11}$$

where V is the amplitude of the voltage across the output of the transformer and R_D is the equivalent input impedance of the lock-in preamplifier paralleled by a parasitic capacitance of the transformer. Typically, R_D was about 6 MΩ when the bridge excitation frequency was 38 Hz.

To within 1% error, the total heat capacity of the sample assembly is proportional to the inverse of the size of temperature oscillations. By comparing our results for this total heat capacity to the data of Kapadnis and Hartmans,[16] we concluded that the background contribution of the heater, thermometer, grease, Kapton film, and crystal lattice to the total heat capacity was less than 10% of the magnetic contribution over the temperature range $1.91 \leq T \leq 2.33$ K ($|\epsilon| \leq 10^{-1}$). Since the background heat capacity is a slowly varying function of temperature, we did not subtract it out before fitting a power-law singularity to the data. Thus this background heat capacity appears as a contribution to the constants B and B' of Eq. (1).

B. Determination of Fitting Parameters

In fitting a power-law singularity [Eq. (1)] to our data, we assume a Gaussian noise distribution with a variance σ^2. Thus the most probable values of the unknown constants T_N, α, α', A, A', B, and B' are those which minimize the quantity[30]

$$\chi^2 = \sum_{\text{data points}} \frac{(C_{\text{data}} - C_{\text{fit}})^2}{\sigma^2 (C_{\text{data}})} . \tag{12}$$

However, we are actually interested in the range of values of T_N, α, and α' for which power-law fits to the data are sufficiently good within the limits of experimental noise. Our procedure is to compute the minimum value of χ^2 corresponding to the values of A and B obtained by the standard linear procedure[31] for specified sets of values of T_N and α for the data points above T_N, and similarly for A', B', T_N, and α' for the points below T_N. The results of these computations can be thought of as a contour map of χ^2 as a function of T_N and α for the data above T_N, and another contour map of χ^2 as a function of T_N and α' for the data below T_N. We use the χ^2 test[32] to determine the maximum value of χ^2 [for each set of data points above T_N and (separately) below T_N] such that any set of parameters yielding a χ^2 greater than this maximum has less than a 10% probability of being the correct parameters. The results are graphically displayed by drawing the contour for the data above T_N (represented by plus signs) with χ^2 equal to the maximum specified by the χ^2 test. Thus the area enclosed by the plus signs (see Fig. 6) represents the range of values for T_N and α allowed by the χ^2 test. Similarly for the data below T_N, the area is outlined by minus signs. The range of values for T_N, α, and α' may be limited further by assuming that the data above and below T_N must be fitted using the same T_N. This range of values is represented by the two shaded areas (see Fig. 6), and is the range of values we conclude fits the data.

There are three possible contributions to our estimate of the variance σ^2. The first comes from the accuracy of the approximations made in Sec. III, which gives a contribution to σ^2 of $10^{-4}C^2$, where C is the total heat capacity. Electronic noise consists of voltage fluctuations which are nearly independent of C, contributing a term to σ^2 proportional to C^4. Temperature fluctuations for the heat sink yield a contribution to σ^2 of $(\Delta T dC/dT)^2$, where ΔT is the amplitude of the temperature fluctuations. This term is negligible except near the transition temperature where the heat capacity is changing rapidly.

From a series of successive measurements (usually three) at each temperature, we computed an approximate σ^2 for the heat-capacity measurement at each temperature. These results were then fitted to an expression of the form $a_2C^2 + a_4C^4$, where a_2 and a_4 are constants. We did not include a term proportional to $(dC/dT)^2$ because an adequate fit was possible without it. Since this did not include errors from the accuracy of the method, we

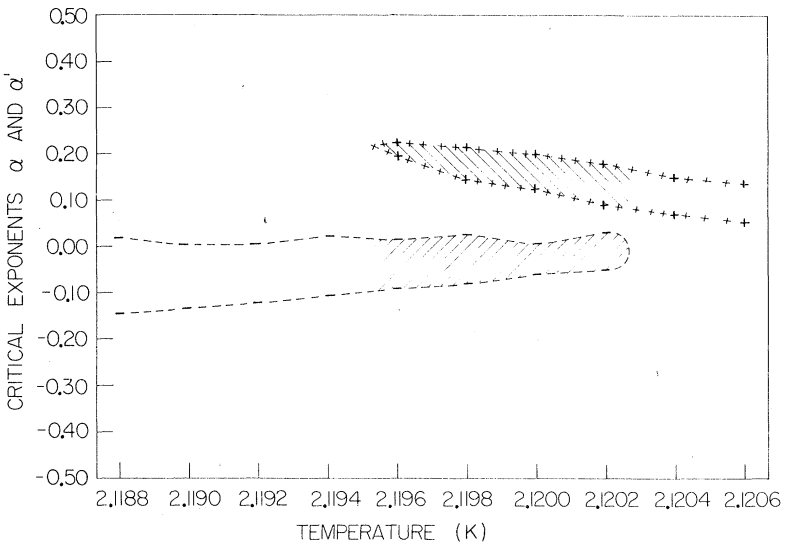

FIG. 6. χ^2-test results for the power-law-singularity fit to the heat-capacity data for $MnBr_2 \cdot 4H_2O$, with $3\times10^{-4} \leq |\epsilon| \leq 10^{-1}$.

increased the value of a_2 to 10^{-4}. Except for the region near the transition, we found σ^2 was dominated by the $10^{-4}C^2$ term. This meant that all data points were nearly evenly weighted by fractional errors.

Because of the effects of rounding and the limited size of the critical region, the data at small $|\epsilon|$ and at large $|\epsilon|$ should not be included in the set of data points used in the fitting. The proper cutoff values of $|\epsilon|$ are not known accurately, so we have repeated the fitting procedure using several different ranges of $|\epsilon|$. The minimum range in $|\epsilon|$ of two decades was chosen because smaller ranges made the uncertainties in the fitting parameters so large as to give meaningless results.

C. Results for Manganese Dibromide Tetrahydrate

The heat capacity of three crystals of $MnBr_2 \cdot 4H_2O$ was measured over the temperature range $1.91 \leq T \leq 2.31$ K, which corresponds to $|\epsilon| \leq 10^{-1}$. Data points were taken approximately evenly spaced on a $\log_{10}|\epsilon|$ temperature scale with about 20 points per decade in $|\epsilon|$ except near the transition temperature, where the data points were approximately evenly spaced on a linear temperature scale with a spacing of about 250 μK. Within experimental error, all three crystals showed the same rounding, which can be seen for one crystal in Fig. 10.

Analyzing the set of data with the least noise, we found that no set of values of T_N, α, and α' fit the data over the entire range in $|\epsilon|$ for which measurements were made within the limits of the χ^2 test. This is a consequence of the rounding at small $|\epsilon|$. By eliminating a half-decade of data near T_N, we were able to fit the remaining data with the results shown in Fig. 6, with the range of values $0.08 \leq \alpha \leq 0.23$; $-0.10 \leq \alpha \leq 0.03$; $2.1195 \leq T_N \leq 2.1203$ K. Eliminating another half-decade of data near T_N gave us the results shown in Fig. 7. Because a smaller range in $|\epsilon|$ was used, there was a larger uncertainty in all three parameters: $0.05 \leq \alpha \leq 0.26$; $-0.18 \leq \alpha' \leq 0.06$; $2.1188 \leq T_N \leq 2.1207$ K. For both the above fits we have assumed that the system has critical singular behavior for $|\epsilon|$ as large as 10^{-1}. It is possible that this is too large a value for $|\epsilon|$. Thus we eliminated a half-decade of data for large $|\epsilon|$ and a half-decade of data at small $|\epsilon|$ and obtained the results shown in Fig. 8. Again, the uncertainty in the parameters was larger than our first fit; however, it is not possible to tell how much of this additional range in values for T_N, α, and α' is caused by the smaller range in $|\epsilon|$ used in the fit and how much results from the possible deviations from critical behavior for $|\epsilon| > 3\times10^{-2}$. The large oscillations in the upper boundary for α' as a function of T_N would seem to indicate that the extension of this upper bound to larger positive values in an artifact of the smaller range in $|\epsilon|$, rather than an indication that critical behavior does not extend to $|\epsilon| = 10^{-1}$. The range of values fitting these data is $0.04 \leq \alpha \leq 0.33$; $-0.11 \leq \alpha' \leq 0.21$; $2.1195 \leq T_N \leq 2.1203$ K.

The expression for the standard deviation squared used in these fits is

$$\sigma^2 = 10^{-4}C^2 + 7\times10^{-6}C^4 . \tag{13}$$

D. Analysis of Dixon-Rives Data for Manganese Dichloride Tetrahydrate

We have reanalyzed the raw data for $MnCl_2 \cdot 4H_2O$ obtained from Dixon and Rives[19] using the same procedure as for our data on $MnBr_2 \cdot 4H_2O$, so that comparisons between these two experiments would reflect actual differences rather than artificial differences introduced by dif-

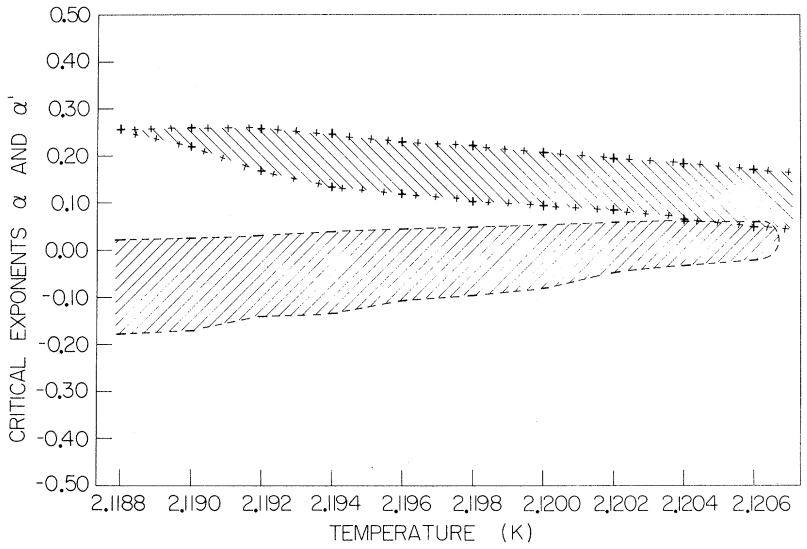

FIG. 7. χ^2-test results for the power-law-singularity fit to the heat-capacity data for $MnBr_2 \cdot 4H_2O$, with $10^{-3} \leq |\epsilon| \leq 10^{-1}$.

ferent fitting procedures.

Since the data of Dixon and Rives were obtained using the adiabatic technique, the data points are more or less evenly spaced on a linear temperature scale. To obtain data points evenly spaced on a $\log_{10}|\epsilon|$ temperature scale, we selected 30 data points per decade in $|\epsilon|$ and averaged any intermediate points with the nearest selected point.

The standard deviation squared for these data was assumed to be proportional to the heat capacity squared. Comparing the resulting χ^2 with our results for $MnBr_2 \cdot 4H_2O$, we concluded that a reasonable valuable is

$$\sigma^2 \cong 1.6 \times 10^{-4} C^2 . \tag{14}$$

Within the χ^2 criterion, we could not fit all of the data with any set of values for T_N, α, and α', again because of the rounding near T_N. If we eliminate all data with $|\epsilon| < 2 \times 10^{-4}$, we obtain the results shown in Fig. 9. From this figure we see that, if we assume the same T_N above and below T_N, the range of values of the fitting parameters is $0.12 \leq \alpha \leq 0.32$; $0.02 \leq \alpha' \leq 0.12$; and $1.6256 \leq T_N \leq 1.6259$ K.

E. Results for Partially Deuterated Manganese Dibromide Tetrahydrate

From susceptibility measurements on normal $MnBr_2 \cdot 4H_2O$ crystals and 96% deuterated crystals, Turrell *et al.*[33] showed a 2.3% shift in the Néel

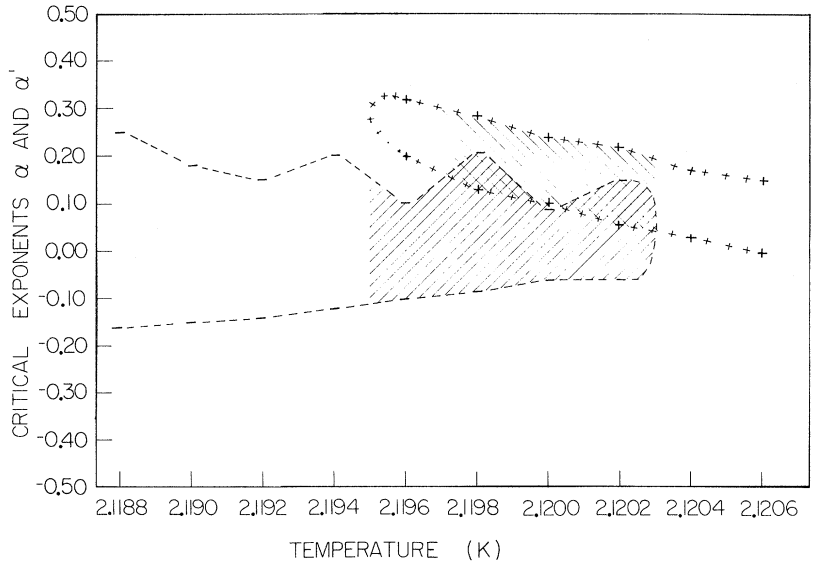

FIG. 8. χ^2-test results for the power-law-singularity fit to the heat-capacity data for $MnBr_2 \cdot 4H_2O$, with $3 \times 10^{-4} \leq |\epsilon| \leq 3 \times 10^{-2}$.

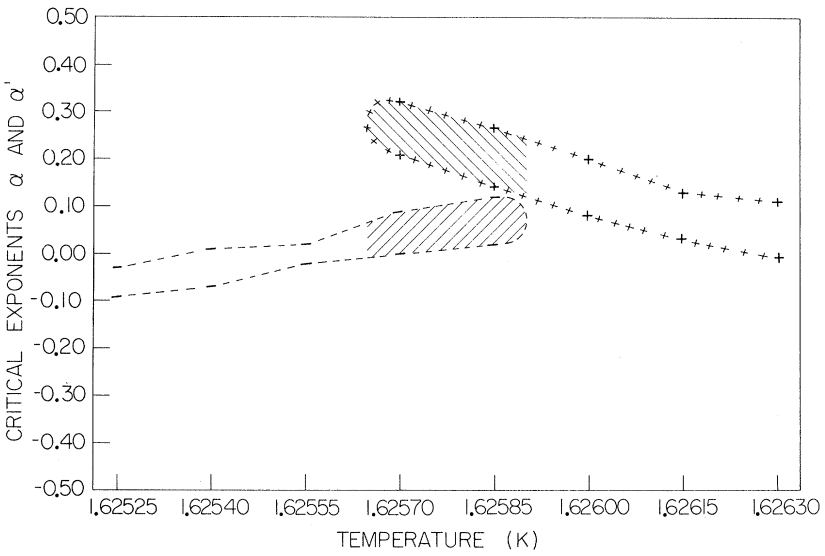

FIG. 9. χ^2-test results for the power-law-singularity fit to the heat-capacity data of Dixon and Rives for $MnCl_2 \cdot 4H_2O$, with $10^{-3} \leq |\epsilon| \leq 2\times10^{-2}$.

temperature showing an alteration in the strength of interaction. In order to see the possible effect of this impurity on the rounding of the heat-capacity singularity, we measured the heat capacity of partially deuterated $MnBr_2 \cdot 4H_2O$ with 1% deuterium. The results in the region of the Néel temperature are shown in Fig. 10 with data for nondeuterated $MnBr_2 \cdot 4H_2O$ superimposed. Within experimental error, we see no significant increase in the rounding.

Because of the improved thermometry, the standard deviation for these data was much less:

$$\sigma^2 = 10^{-4}C^2 \cdot \qquad (15)$$

Furthermore, within the χ^2 test we were unable to obtain fits for data in the range $3\times10^{-4} \leq |\epsilon| \leq 10^{-1}$. The results of fitting to the data in the range $10^{-3} \leq |\epsilon| \leq 10^{-1}$ are shown in Fig. 11. From this figure we see that $0.01 \leq \alpha \leq 0.21$; $-0.10 \leq \alpha' \leq 0.10$; and $2.1188 \leq T_N \leq 2.1204$ K.

In Fig. 12 we show the logarithm of the heat capacity plotted vs $\log_{10}|\epsilon|$, where the value $T_N = 2.1196$ K was used to compute $|\epsilon|$. The solid curves represent the fitting functions which just satisfy the χ^2 criterion.

V. DISCUSSION OF RESULTS

We can compare our fitting results for α and α' to the series-expansion calculations.[3] From the results of Jasnow and Wortis[34] and of Riedel and

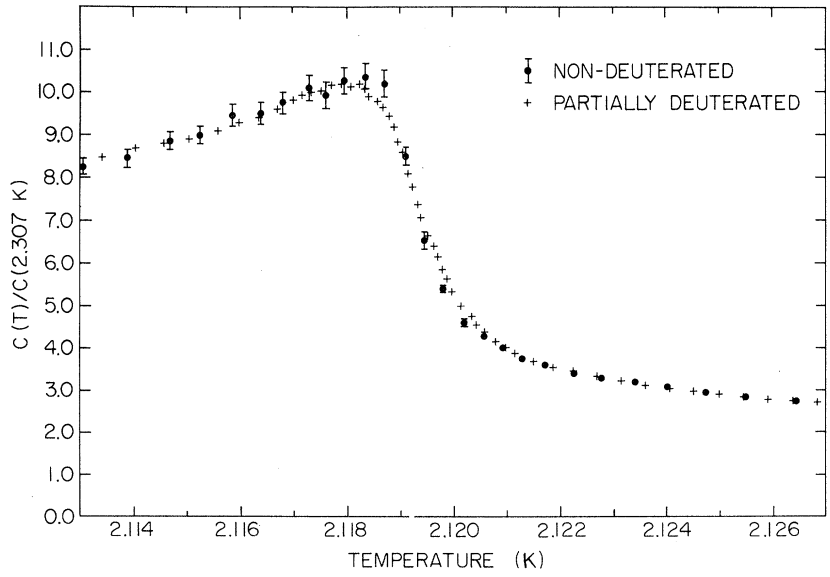

FIG. 10. Heat-capacity data for partially deuterated $MnBr_2 \cdot 4H_2O$ near its transition temperature compared to data for nondeuterated $MnBr_2 \cdot 4H_2O$ (latter data shifted in temperature to compare rounding).

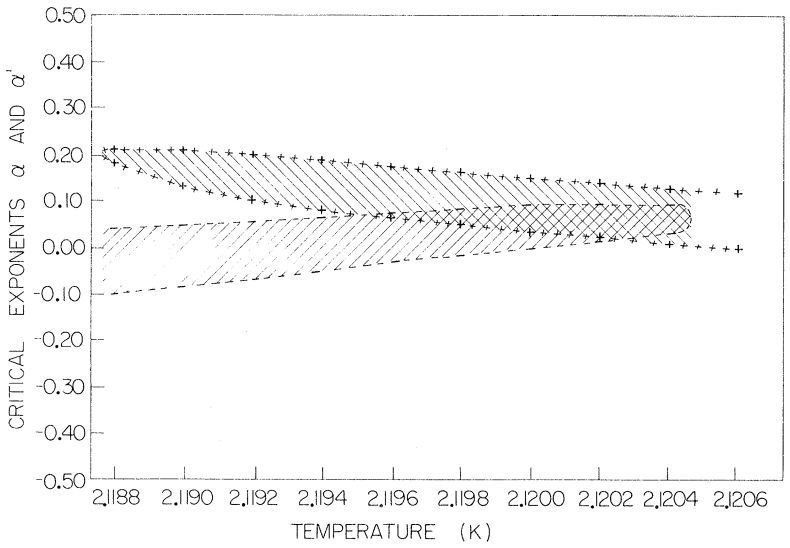

FIG. 11. χ^2-test results for the power-law-singularity fit to heat-capacity data for 1% deuterated $MnBr_2 \cdot 4H_2O$, with $10^{-3} \leq |\epsilon| \leq 10^{-1}$.

Wegner,[35] we expect α and α' to be Ising-like, since the magnetic-dipole interactions induce a uniaxial anisotropy. Since the magnetic interactions are not nearest-neighbor only, we expect from the results of Domb and Dalton[36] that the effect of further-neighbor interactions is to reduce the largest value of $|\epsilon|$ for which the critical singularity dominates the heat capacity. However, the work of Joyce[37] indicates that the effect of the long-range nature of the magnetic-dipole interactions may be to alter the values of α and α' found in the Ising model. Finally, the work of Domb and Sykes[38] indicates that the effect of the spin $\frac{5}{2}$ of the manganese ions compared to the spin $\frac{1}{2}$ used in most Ising-model calculations may be to increase the value of α. The effect on α' is not known.

The best-fitting results for $MnBr_2 \cdot 4H_2O$ are those shown in Fig. 6, from which we conclude that $0.01 \leq \alpha \leq 0.21$ and $-0.10 \leq \alpha' \leq 0.10$. This result for α compares favorably with the three-dimensional spin-$\frac{1}{2}$ Ising-model series-expansion results for a face-centered-cubic lattice: $0.10 \leq \alpha \leq 0.14$.[39] However, this result for α is not consistent with the series-expansion results for the three-dimensional face-centered-cubic Heisenberg model for spin $\frac{1}{2}$: $-0.25 \leq \alpha \leq -0.15$,[40] or for spin ∞: $-0.20 \leq \alpha \leq -0.00$.[41] Our result for α' compares less favorably than α with the three-dimensional spin-$\frac{1}{2}$ Ising-model series-expansion results for a face-centered-cubic lattice: $0.026 \leq \alpha' \leq 0.226$.[42]

We can also compare our results to the scaling-law prediction[43]:

$$\alpha = \alpha' .$$

From our best results for α and α' we conclude that the scaling-law prediction may be correct. However, our data would seem to indicate that α is somewhat larger than α'.

Comparing our results for $MnBr_2 \cdot 4H_2O$ with our fitting results of Dixon-Rives data for $MnCl_2 \cdot 4H_2O$, we see that they are very similar and have a high probability of having equal values for α and for α'. If we were to compare our *fitting* results for the

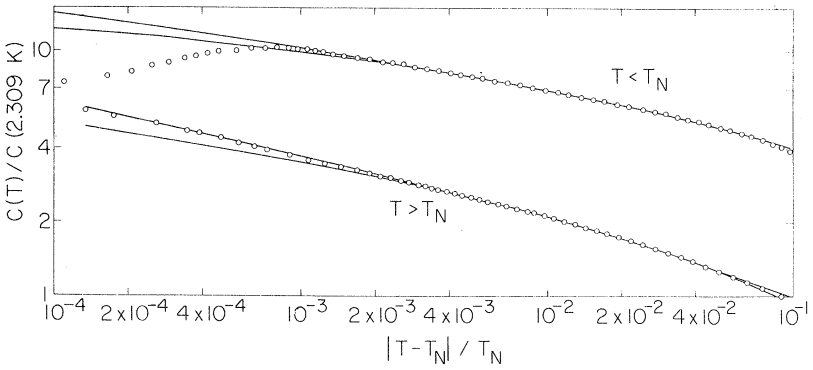

FIG. 12. Heat-capacity data for 1% deuterated $MnBr_2 \cdot 4H_2O$ on a $\log_{10}|\epsilon|$ temperature scale, with $T_N = 2.119600$ K, compared to several power-law-fitting functions.

bromide with Dixon and Rives's *fitting* results for the chloride ($\alpha \cong 0.35$; $\alpha' \cong 0.0$), we would have concluded that α was larger for the chloride than for the bromide. We make no special claims for our fitting procedure; however, we believe that our study shows that comparisons between *fitting* results for different materials can be misleading when different fitting procedures are used. This conclusion also applies to a comparison of our heat-capacity measurements with the thermal-expansion measurements of Philip *et al.*,[6] especially since Philip *et al.* appear to set T_N at the maximum of the singularity.

We summarize the results of the critical exponents using our fitting procedure along with the results for the Ising and Heisenberg models in Table I.

We have found that the heat-capacity singularities of our crystals of $MnBr_2 \cdot 4H_2O$ are rounded over the region $|\epsilon| \lesssim 3\times 10^{-4}$. There are many possible sources of this rounding, including chemical impurities, crystalline imperfections, isotopic impurities, and thermal distortion of the lattice at the transition temperature.

McCoy and Wu[44] have tried to find the effect of random impurities by a study of a two-dimensional Ising model on a rectangular lattice with constant interactions in one direction and randomly varying interactions in the other direction. Because of the complexity of their functional form for the heat capacity and the lack of any relation between their random variation in interaction strength with the impurity concentration, we have not tried to fit their functional form to our data.

Fisher and Ferdinand[45] have calculated exactly the interfacial and boundary free energies for various two-dimensional Ising lattices. They interpret their results in terms of the rounding and displacement of the heat-capacity maximum. The rounding should begin when the spin-spin correlation length reaches the size of the mean linear dimensions or, if applied to impurities, the mean interimpurity distance. From Fisher and Burford,[46] for rounding at $|\epsilon| \sim 3\times 10^{-4}$, we expect that the spin-spin correlation length is limited to about 200 spin spacings. Since this is comparable to the typical interimpurity distance for chemical impurities of 140 spin spacings, our results are consistent with Fisher and Ferdinand's model. However, in the partially deuterated crystals the average distance between heavy-water molecules along a line is 25 spin spacings. From the above we would expect rounding at $|\epsilon| \sim 2\times 10^{-3}$. However, since we observe no increased rounding, either deuterium is too weak an impurity or the above model is not valid.

Baker and Essam[47] have analyzed the effects of lattice compressibility on the specific-heat singularity for a compressible Ising lattice with a rigid constraint on the surface spins. They find that the model satisfies Fisher's criteria[48] in deriving the critical-exponent renormalization. Using the values for the three-dimensional face-centered-cubic spin-$\frac{1}{2}$ Ising model, their model predicts

$$\alpha' = 0.071^{+0.044}_{-0.221}, \tag{16}$$

$$\alpha = -0.143 \pm 0.020 . \tag{17}$$

Although our results for α' satisfy their prediction, the results for α clearly do not. Therefore, we have not tried to fit our data to their functional form for the specific heat at constant pressure.

Wagner[49] has used a unitary transformation to decouple the spin system from the lattice. Using a droplet model[3] for temperatures below the transition temperature, he finds that a critical reduced temperature $|\epsilon|_c$ exists such that the specific-heat singularity is unaffected for $|\epsilon| \gg |\epsilon|_c$, but for $|\epsilon| \ll |\epsilon|_c$ the heat capacity approaches a finite value linearly with $|\epsilon|$ as $|\epsilon| \to 0$. Using Wagner's expression for $|\epsilon|_c$, we find $|\epsilon|_c \sim 5\times 10^{-8}$ for $MnBr_2 \cdot 4H_2O$.[15] Thus this model predicts a rounding at a much smaller value of $|\epsilon|$ than observed.

TABLE I. Critical exponents.

Materials	Range of $\lvert\epsilon\rvert$	Range of α	Range of α'
	3×10^{-4}–10^{-1}	0.08 – 0.23	−0.10 – 0.03
$MnBr_2 \cdot 4H_2O$	10^{-3}–10^{-1}	0.05 – 0.26	−0.18 – 0.06
	3×10^{-4}–3×10^{-2}	0.04 – 0.33	−0.11 – 0.21
1% deuterated $MnBr_2 \cdot 4H_2O$	10^{-3}–10^{-1}	0.01 – 0.21	−0.10 – 0.10
$MnCl_2 \cdot 4H_2O$	2×10^{-4}–2×10^{-2}	0.12 – 0.32	0.02 – 0.12
Model			
3-dim. fcc spin = $\frac{1}{2}$ Ising		0.10 – 0.14	0.026 – 0.226
3-dim. fcc spin = $\frac{1}{2}$ Heisenberg		−0.25 – 0.15	...
3-dim. fcc spin = ∞ Heisenberg		−0.20 – 0.00	...

VI. CONCLUSIONS

Even with the increased precision of heat-capacity measurements available from the oscillating-temperature technique, the uncertainties in α and α' are still very large. This is due to the presence of rounding and the uncertainty in the range of $|\epsilon|$ over which the heat capacity obeys a power-law singularity. We have shown that the rounding present in a small single crystal is not less than for a large single crystal. Furthermore, the rounding is not influenced by the presence of deuterium isotopes in the waters of hydration in concentrations up to 1%. The rounding is consistent with the model of Fisher and Ferdinand,[45] where the spin-spin correlation length is limited by the chemical impurities.

ACKNOWLEDGMENTS

The authors would like to thank Dr. Dan Zally for providing the germanium thermometers and Dr. V. G. Mossotti for the quantitative analysis of samples. Professor John Rives and Dr. George Dixon are thanked for providing their raw data. Professor Myron Salamon, Professor Michael Wortis, and Dr. P. C. Hohenberg were helpful on various theoretical aspects. Finally, one of the authors (R. D. H.) thanks the National Science Foundation, Eastman Kodak Corp., and the General Dynamics Corp. for fellowship support.

---

*Work supported in part by the Advanced Research Projects Agency under Contract No. HC 15-67-C-0221.

†Based on the Ph. D. thesis of R. D. Hempstead (University of Illinois, 1970) (unpublished).

‡Present address: IBM Research Center, Yorktown Heights, N. Y. 10598.

[1]L. P. Kadanoff, W. Götze, D. Hamblen, R. Hecht, E. A. S. Lewis, V. V. Palciauskas, M. Rayl, J. Swift, D. Aspnes, and J. Kane, Rev. Mod. Phys. 39, 395 (1967); P. Heller, Rept. Progr. Phys. 30, 731 (1967).

[2]J. Ashman and P. Handler, Phys. Rev. Letters 23, 642 (1969). Rather than using the constants A, B, A', and B', they are able to fit their data to the series-expansion result for the bcc-lattice three-dimensional ($S=\frac{1}{2}$) Ising model, which has slowly varying functions of temperature instead of B and B'.

[3]See M. E. Fisher, Rept. Progr. Phys. 30, 615 (1967), for a review.

[4]See L. P. Kadanoff, Wolfgang Götze, David Hamblen, Robert Hecht, E. A. S. Lewis, V. V. Palciauskas, Martin Rayl, J. Swift, David Aspnes, and Joseph Kane, Rev. Mod. Phys. 39, 395 (1967), Chap. II, Sec. F, for a discussion of the breakdown of the Landau theory indicating the region of $|\epsilon|$ where fluctuations are dominant.

[5]Recent work by J. H. Schelleng and S. A. Friedberg [Phys. Rev. 185, 728 (1969)] suggests that the magnetic structure of $MnBr_2 \cdot 4H_2O$ may not be identical to $MnCl_2 \cdot 4H_2O$.

[6]J. W. Philip, R. Gonano, and E. D. Adams, Phys. Rev. 188, 973 (1969).

[7]W. E. Henry, Phys. Rev. 94, 1146 (1954).

[8]A. Zalkin, J. D. Forrester, and D. H. Templeton, Inorg. Chem. 3, 529 (1964).

[9]R. D. Spence and V. Nagarajan, Phys. Rev. 149, 191 (1966).

[10]H. M. Gijsman, N. J. Poulis, and J. Van den Handel, Physica 25, 954 (1959).

[11]T. Nagamiaja, K. Yosida, and R. Kubo, Advan. Phys. 4, 1 (1955).

[12]J. H. Schelleng and S. A. Friedberg, Phys. Rev. 185, 728 (1969); V. A. Schmidt and S. A. Friedberg, J. Appl. Phys. 38, 5319 (1967).

[13]B. Bolger, in *Conference de Physique des Basses Temperatures, Paris*, 1955 (Centre Nationale de la Recherche Scientifique and UNESCO, Paris, 1956), p. 244.

[14]I. Tsujikawa and E. Kanda, J. Phys. Radium 20, 352 (1959); J. Phys. Soc. Japan 18, 1382 (1963).

[15]See R. D. Hempstead [Ph. D. thesis (University of Illinois, 1970) (unpublished)] for details of this comparison.

[16]D. G. Kapadnis and R. Hartmans, Physics 22, 181 (1956).

[17]J. H. Schelleng and S. A. Friedberg, J. Appl. Phys. 34, 1087 (1963); Phys. Rev. 185, 728 (1969).

[18]A. R. Miedema, R. F. Wielinga, and W. J. Huiskamp, Physica 31, 835 (1965).

[19]G. S. Dixon and J. E. Rives, Phys. Rev. 177, 871 (1969).

[20]E. Callen and H. B. Callen, Phys. Rev. 139, A455 (1965).

[21]See Sec. III of Ref. 6 for a review of this work.

[22]P. Sullivan and G. Seidel, Ann. Acad. Sci. Fennicae 210, 58 (1966); Phys. Letters 25A, 229 (1967); Phys. Rev. 173, 679 (1968). This method was first used at high temperatures by P. Handler, D. E. Mapother, and M. Rayl, Phys. Rev. Letters 19, 356 (1967).

[23]See, for example, J. Skalyo, Jr. and S. A. Friedberg, Phys. Rev. Letters 13, 133 (1964).

[24]See, for example, B. E. Keen, D. P. Landau, and W. P. Wolf, J. Appl. Phys. 38, 967 (1967); D. T. Teaney, Phys. Rev. Letters 14, 898 (1965).

[25]100-KΩ precision-wire-wound resistor type WW4J manufactured by IRC Corp.

[26]The source of this excessive noise was not identified; however, it may have been in the contacts. Contacts on commercial germanium thermometers are made by gold plating the contact area on the germanium and spot welding gold wires to that area. See J. E. Kunzler, T. H. Geballe, and G. W. Hull, Rev. Sci. Instr. 28, 96 (1957), for details of construction.

[27]A. C. Anderson, R. B. Rauch, and M. M. Kreitman, Rev. Sci. Instr. 41, 469 (1970).

[28]This functional form was taken from R. E. Harris, Technical Report No. 1, U. S. Army Research Office (Durham) Project No. DA-ARO(D)-31-124-G-343.

[29]J. S. Blakemore, J. W. Schultze, and J. G. Myers, Rev. Sci. Instr. 33, 545 (1962).

[30]J. Mathews and R. L. Walker, *Mathematical Methods of Physics* (Benjamin, New York, 1965), Sec. 14-6.

[31]F. B. Hildebrand, *Introduction to Numerical Analysis* (McGraw-Hill, New York, 1956), Chap. 7.

[32]P. R. Bevington, *Data Reduction and Error Analysis for the Physical Sciences* (McGraw-Hill, New York, 1969), Chap. 5; see also Ref. 31.
[33]B. G. Turrell, C. L. Yue, and S. D. Sahri, Phys. Letters 28A, 680 (1969).
[34]D. Jasnow and M. Wortis, Phys. Rev. 176, 739 (1968).
[35]E. Riedel and F. Wegner, Z. Physik 225, 195 (1969).
[36]C. Domb and N. W. Dalton, Proc. Phys. Soc. (London) 89, 859 (1966); 89, 873 (1966); N. W. Dalton, Ph. D. thesis (University of London) (unpublished); Proc. Phys. Soc. (London) 90, 459 (1966).
[37]G. S. Joyce, Phys. Rev. 146, 349 (1966).
[38]C. Domb and M. F. Sykes, Phys. Rev. 128, 168 (1962).
[39]M. F. Sykes, J. L. Martin, and D. L. Hunter, Proc. Phys. Soc. (London) 91, 671 (1967).
[40]G. A. Baker, Jr., H. E. Gilbert, J. Eve, and G. S. Rushbrooke, Phys. Rev. 164, 800 (1967).
[41]D. Jasnow and M. A. Moore, Phys. Rev. 176, 751(1968).
[42]G. A. Baker, Jr. and D. S. Gaunt, Phys. Rev. 155, 545 (1967).
[43]B. Widom, J. Chem. Phys. 43, 3892 (1965); 43, 3898 (1965); L. P. Kadanoff, Physics 2, 263 (1966); M. E. Fisher, J. Appl. Phys. 38, 981 (1967).
[44]B. M. McCoy and T. T. Wu, Phys. Rev. Letters 21, 549 (1968); Phys. Rev. 176, 631 (1968).
[45]M. E. Fisher and A. E. Ferdinand, Phys. Rev. Letters 19, 169 (1967); A. E. Ferdinand and M. E. Fisher, Phys. Rev. 185, 832 (1969).
[46]M. E. Fisher and R. J. Burford, Phys. Rev. 156, 583 (1967).
[47]G. A. Baker and J. W. Essam, Phys. Rev. Letters 24, 447 (1970).
[48]M. E. Fisher, Phys. Rev. 176, 257 (1968).
[49]H. Wagner, Phys. Rev. Letters 25, 31 (1970).

PHYSICAL REVIEW B VOLUME 7, NUMBER 1 1 JANUARY 1973

Cyclotron Resonance in Nickel

P. Goy
École Normale Supérieure, Paris, France

and

C. C. Grimes
Bell Laboratories, Murray Hill, New Jersey 07974
(Received 2 August 1972)

Azbel–Kaner cyclotron resonance was studied at 277 GHz and 1.5 °K in a (100)-plane single-crystal specimen of Ni. Resonances from both the neck and belly of the Cu-like majority-spin s-p–band Fermi surface were seen. The neck yielded $m^*/m_0 = 0.35 \pm 0.014$ when $\vec{H}$ was along ⟨011⟩. Beat structure in the subharmonic resonances suggested that belly orbits on both the majority- and minority-spin s-p–band Fermi surfaces were observed for $\vec{H}$ within 28° of ⟨001⟩. As $\vec{H}$ was rotated away from ⟨001⟩ the heavier mass increased smoothly from $m^*/m_0 = 5.09$ to 5.9 while the lighter mass increased from 4.33 to 4.86. Only one of the three pairs of symmetry-related minority-spin d-band hole pockets were seen. The pockets having their greatest dimension along ⟨001⟩ yielded an effective mass which increased from $m^*/m_0 = 0.75 \pm 0.03$ at ⟨001⟩ to $m^*m_0 = 1.11$ when $\vec{H}$ was 34° from ⟨001⟩.

I. INTRODUCTION

We report the first experimental study of Azbel–Kaner cyclotron resonance in a ferromagnetic metal. This study, in the {100} plane of Ni, has yielded effective masses from $0.35m_0$ to $7.5m_0$, where m_0 is the free-electron mass. The variations of the effective masses with magnetic field orientation are consistent with a model Fermi surface for Ni proposed by Hodges, Ehrenreich, and Lang.[1,2] Using their model Fermi surface, the observed resonances are identified as arising from orbits around the central sections of the s-p–band Fermi surfaces as well as orbits around the smaller sections of Fermi surface which were observed earlier by others in de Haas–van Alphen-effect (dHvA) studies.

In the remaining paragraphs of this section we describe the model Fermi surface (FS) of Hodges *et al.* In Sec. II, we give a brief account of the experimental details. Our experimental results are presented in Sec. III together with our identification of each observed effective mass with an orbit around the FS. Additional implications of our results are discussed in Sec. IV. A summary and acknowledgments then complete this work.

The current itinerant-electron or band model of the electronic structure of nickel has grown out of an interplay between theory and experiment. The high-field galvanomagnetic studies of Fawcett and Reed showed that both the s-p and d electrons form bands with a net conduction-electron density of one electron per atom, and that one sheet of the FS has necks in the ⟨111⟩ directions like the well-known FS of copper.[3] The necks in Ni were observed in dHvA studies by Joseph and Thorsen.[4]